Supporting Information

Taschenberger et al. 10.1073/pnas.1606383113

SI Text

The Parallel Two-Pool Model. For a simple quantitative description of our results we assume that resting synapses have a pool of SV_ns, which is similar in size among synapses. SV_ns are released during an AP with release probability p_n. The SV_n pool, when fully loaded, has the size N_n. In addition, individual synapses have a pool of SV_ss of variable size, which has a size $\alpha \times N_n$. Here, α is a constant for a given synapse, representing the abundance of sites for SV_ss. α increases in response to PdBu application or during induction of PTP. SV_ss are released with higher release probability, which is $\beta \times p_n$. Thus, the total quantal content m_1 of the first EPSC in response to a stimulus train is

$$m_1 = N_n \cdot p_n \cdot (1+\alpha'), \qquad \textbf{[S1]}$$

where α' was substituted for $\alpha \times \beta$. During stimulus trains release probability may change and pools get partially depleted. For simplicity, we assume that relative changes in release probability are the same for SV_ns and SV_ss. They are characterized by the factor $\varepsilon(f)$, which is defined as the ratio of p_n of the first stimulus over that at steady state. $\varepsilon(f)$ is a function of stimulation frequency f, which most likely is close to 1, except for the highest frequencies (100 Hz and 200 Hz). We include $\varepsilon(f)$ in the equations here for completeness, but make the simplifying assumption $\varepsilon(f) = 1$ in most instances, except when discussing the time course of the SV_s and SV_n components of EPSCs. Steady-state depletion of pools is also a function of frequency, which we denote with $\gamma(f)$ for SV_ns and $\delta(f)$ for SV_ss. The functions $\varepsilon(f)$, $\gamma(f)$, and $\delta(f)$ thus represent facilitation and short-term depression of SVs. With these definitions the steady-state quantal content m_{ss} is

$$m_{ss} = N_n \cdot p_n \cdot \varepsilon(f) \cdot [\gamma(f) + \alpha' \cdot \delta(f)]. \qquad \textbf{[S2]}$$

In plots like that of Fig. 3*C* different synapses are assumed to differ only in α'. For the discussion of such plots it is convenient to introduce their y and x coordinates as $x_i = q \times m_{1,i}$ and $y_i = q \times m_{ss,i}$, where q is the quantal size, the subscript i denotes a given synapse, and ss refers to steady state. Also, we define the coordinates x_n and y_n for (hypothetical!) synapses with $\alpha' = 0$ as

$$y_n = q \cdot N_n \cdot p_n \cdot \varepsilon(f) \cdot \gamma(f) \qquad \textbf{[S3]}$$

$$x_n = q \cdot N_n \cdot p_n. \qquad \textbf{[S4]}$$

With these definitions, using **[S1]** and **[S2]** we obtain

$$y - y_n = \varepsilon(f) \cdot \delta(f) \cdot (x - x_n). \qquad \textbf{[S5]}$$

For a given frequency this is a straight line, passing through (y_n, x_n), with slope $\varepsilon(f) \times \delta(f)$. Thus, the slopes of line fits in Fig. 3*C* provide the pool depletion factors of SV_ss, multiplied by a facilitation factor. Likewise, considering **[S3]** and **[S4]**, the ratio y_n/x_n is the product $\varepsilon(f) \times \gamma(f)$, providing the pool depletion factors of SV_ns, again multiplied by possible influence of facilitation. In the main text we assumed $\varepsilon(f) = 1$ for simplicity, which should be valid for low frequencies. However, for frequencies ≥50 Hz, there are clear indications for $\varepsilon(f) > 1$. (see *Results* for the time course of the SV_s component.) The y-axis intercept, y_0, of the line fit according to Eqs. **S3**–**S5** is

$$y_0 = x_n \cdot (\varepsilon(f) \cdot \gamma(f) - \varepsilon(f) \cdot \delta(f)). \qquad \textbf{[S6]}$$

In this equation $\varepsilon(f) \times \delta(f)$ and y_0 are known, such that it establishes a relationship between $\varepsilon(f) \times \gamma(f)$ and x_n. Thus, we cannot determine any of the two quantities individually. If, however, an assumption is made for one of them, for instance $0.8 < \varepsilon(f) \times \gamma(f) < 1$, we can determine upper and lower bounds for x_n. Using a 1-Hz line fit to control data [$y_0 = -0.152$ nA; $\delta(1) = 0.489$] and assuming $\varepsilon(f) = 1$, we obtain

$$-0.29 \text{ nA} > x_n > -0.49 \text{ nA}. \qquad \textbf{[S7]}$$

This result confirms the qualitative conclusions in the main text about the size of the SV_n pool under the likely assumption, that for all frequencies ≤1 Hz there is neither appreciable facilitation nor depletion of the SV_n pool, unless there are compensatory changes.

Kinetics of Priming. For a quantitative analysis of priming processes (normal priming and superpriming) we make the simplest possible assumption, namely that both SV pools are consumed and refilled independently according to a first-order reaction scheme

$$\xrightarrow{k_{+,i}} \text{pool}_i \xrightarrow{p_i \cdot f}. \qquad \textbf{[S8]}$$

Here, $k_{+,i}$ are the rate constants of refilling of the respective pool and $p_i \times f$ is the product of frequency and release probability (i refers to either the superprimed or the nonsuperprimed pool). This leads to the equation

$$\text{Pool}_{i,ss} = \text{Pool}_{i,0} \cdot \frac{k_{+,i}}{k_{+,i} + p_i \cdot f}, \qquad \textbf{[S9]}$$

where the subscript ss refers to steady state. Writing this equation for the two pools considered here, with the definition of p_n, including its frequency dependence $\varepsilon(f)$ (Eq. **S1**), and introducing the definitions

$$f_n = \frac{k_{+n}}{p_n \cdot \varepsilon(f)} \quad f_s = \frac{k_{+s}}{p_n \cdot \beta \cdot \varepsilon(f)}, \qquad \textbf{[S10]}$$

we obtain from **[S3]**, **[S4]**, **[S9]**, and **[S10]**

$$y_n / x_n = \varepsilon(f) \cdot \gamma(f) = \frac{\varepsilon(f)}{1 + f/f_n}, \qquad \textbf{[S11]}$$

and for the slope $s(f)$ of Fig. 3*C*

$$s(f) = \varepsilon(f) \cdot \delta(f) = \frac{\varepsilon(f)}{1 + f/f_s}. \qquad \textbf{[S12]}$$

The fit of Fig. 4*B* was calculated according to Eqs. **S10** and **S12**, once for a fixed value of $k_{+,s}$ of 0.8 s^{-1} and once for a frequency-dependent one:

$$k_{+,s} = 0.5 \text{ s}^{-1} + 1.9 \cdot \frac{f}{f + 15 \text{ s}^{-1}}.$$

$\varepsilon(f)$ was assumed to be 1, which is expected to hold, except for the highest frequencies of 100 Hz and 200 Hz.

SI Materials and Methods

Slice Preparation. Juvenile, posthearing (P13–16) Wistar rats of either sex were used for most experiments. Brainstem slices were

prepared as previously described (35). In short, after decapitation, the whole brain was immediately immersed into ice-cold low Ca^{2+} artificial CSF (aCSF) containing 125 mM NaCl, 2.5 mM KCl, 3 mM $MgCl_2$, 0.1 mM $CaCl_2$, 10 mM glucose, 25 mM $NaHCO_3$, 1.25 mM NaH_2PO_4, 0.4 mM ascorbic acid, 3 mM myo-inositol, and 2 mM Na-pyruvate, pH 7.3, when bubbled with carbogen (95% O_2, 5% CO_2). The brainstem was glued onto the stage of a VT1000S vibratome (Leica) and 200-μm thick coronal slices containing the MNTB were cut. Slices were incubated for 30–40 min at 35 °C in an incubation chamber containing normal aCSF and kept at room temperature (22–24 °C) for up to 4 h thereafter. The composition of normal aCSF was identical to that of low Ca^{2+} aCSF except that 1.0 mM $MgCl_2$ and 2.0 mM $CaCl_2$ were used.

Electrophysiology. Whole-cell patch-clamp recordings were made from calyx of Held terminals and principal neurons of the MNTB, using an EPC-10 amplifier controlled by Pulse software (HEKA Elektronik). Sampling intervals and filter settings were 20 μs and 5.0 kHz, respectively. Cells were visualized by infrared-differential interference contrast microscopy through a 40× water-immersion objective, using an upright microscope (Olympus BX51WI). During experiments, slices were continuously perfused with normal aCSF solution. All experiments were carried out at room temperature (22–24 °C). For postsynaptic recordings, patch pipettes were pulled from thin-walled glass (World Precision Instruments) on a PIP-5 puller (HEKA Elektronik). Open tip resistance was 2.5–3.5 MΩ. R_s ranged from 4 MΩ to 7 MΩ. R_s compensation was set to ≥84% (2 μs delay). The holding potential was −70 mV. Pipettes were filled with a solution consisting of the following: 140 mM Cs-gluconate, 20 mM TEA-Cl, 10 mM Hepes, 5 mM EGTA, 5 mM Na_2-phosphocreatine, 5 mM ATP-Mg, 0.3 mM GTP, pH 7.3, with CsOH. No corrections were made for liquid junction potentials.

EPSCs were elicited by afferent fiber stimulation via a bipolar stimulation electrode placed halfway between the brainstem midline and the MNTB. Stimulation pulses (100 μs duration) were applied using a stimulus isolator unit (AMPI), with the output voltage set to 1–2 V above threshold for AP generation (≤25 V) to exclude stimulation failures at higher frequencies. For each AP-evoked EPSC the series resistance (R_s) value was updated and stored with the data, using the automated R_s compensation routine implemented in Pulse. Postsynaptic recordings with a leak current >300 pA were excluded from the analysis. For clarity, stimulation artifacts were blanked for the EPSCs displayed in Figs. 1 and 5.

A total of 1 mM kynurenic acid was added to the bath solution to minimize AMPAR desensitization and saturation in the experiments illustrated in Figs. 1–5. Nevertheless, indications of residual desensitization were apparent in some recordings, particularly in those with large EPSCs. For instance, in Fig. 5*D* the line fits to data from PTP experiments intersect at smaller initial EPSC amplitudes than those in Fig. 3*C*. This result is most likely due to differences in slope of the line fits to the 100-Hz scatter plots. Desensitization in strongly potentiated synapses may be the cause for a negative slope of the plot in Fig. 5*D*. (For another indication of desensitization see Fig. 4*A* legend.)

In Fig. 5 *A* and *C* data are presented for four time intervals, relative to the induction of PTP. For EPSC trains without preconditioning these time intervals were selected as follows: before, average of five trains immediately before induction of PTP; early, average of two trains at 45 s and 75 s after tetanus onset; medium, average of three trains at 105 s, 135 s, and 165 s after tetanus onset; and late, average of three trains at 255 s, 285 s, and 315 s after tetanus onset.

Preconditioned 100-Hz trains were acquired 15 s earlier than the respective values given above.

Offline analysis was performed using Igor Pro (Wavemetrics). Remaining series-resistance errors were corrected (67) using the R_s values stored in the data files (assuming a linear IV relationship with a reversal potential of +10 mV). EPSCs were subsequently offset corrected and low-pass filtered (f_{cutoff} = 5 kHz), using a 10-pole software Bessel filter. Original data are presented as mean ± SEM. SDs of fitting parameters are given, as supplied by Igor Pro curve-fitting algorithms. For derived quantities (products, ratios, etc.) SEM was calculated assuming Gaussian error propagation.

Glutamate Sensor and Optical Recordings. Primary hippocampal cultures were prepared from 1-d-old Wistar rats according to the regulations of the Max Planck Society and plated on poly-D-lysine–coated coverslips. Calcium phosphate-mediated transfection of neurons with iGLuSnFR (Addgene plasmid 41732) was performed at 3 DIV. All imaging experiments were performed at DIV 14–21 at room temperature (22–24 °C). During measurements neurons were perfused with modified Tyrode's solution (140 mM NaCl, 2.5 mM KCl, 3 mM $CaCl_2$, 1 mM $MgCl_2$, 10 mM glucose, 10 mM Hepes, pH 7.4). A total of 10 μM 6-cyano-7-nitroquinoxaline-2, 3-dione (CNQX) and 50 μM D, l-2-amino-5-phosphonovaleric acid (AP5) were added to prevent recurrent activity.

Coverslips were mounted in a custom imaging chamber on the stage of a Nikon TE2000 inverted microscope. iGluSnFR fluorescence was excited with a 488-nm diode laser (Coherent) and emission was imaged with a Zyla 5.5 sCMOS camera (Andor Technology) at 100 Hz through a 60×, 1.2 NA Plan Apo objective, using a 510-nm dichroic and 515–560-nm emission filter. Action potentials were evoked by 1-ms current pulses (WPI A 385; World Precision Instruments), yielding a 10 V/cm field between two platinum electrodes. Timing of stimuli was controlled by a Master 8 pulse generator and triggered by computer-controlled TTL output. Image acquisition and hardware synchronization were controlled by Andor IQ2. Image analysis was performed in Matlab.

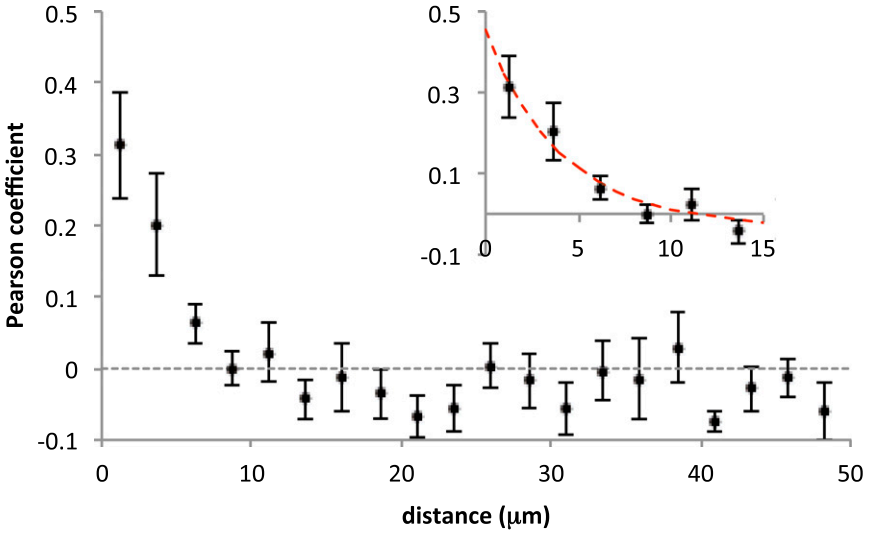

Fig. S1. Spatial correlation of PPR between neighboring boutons. Release site pairs were grouped into 2.5-μm bins and cross-correlation of corresponding PPR values was performed. The mean ± SEM of correlation coefficients recovered from all measurements ($n = 9$) is plotted for pairs up to 50 μm apart. The decay of correlation with increasing distance was fitted with a single exponential (*Inset*) and a PPR correlation length constant of 4.1 μm (95% confidence interval: 2.6, 5.7) was determined. Error bars indicate SD.